

# Set Voronoi Tessellation for Particulate Systems in Two Dimensions

Simeon Völkel and Kai Huang

**Abstract** Given a countable set of points in a continuous space, Voronoi tessellation is an intuitive way of partitioning the space according to the distance to the individual points. As a powerful approach to obtain structural information, it has a long history and widespread applications in diverse disciplines, from astronomy to urban planning. For particulate systems in real life, such as a pile of sand or a crowd of pedestrians, the realization of Voronoi tessellation needs to be modified to accommodate the fact that the particles cannot be simply treated as points. Here, we elucidate the use of Set Voronoi tessellation (i. e., considering for a non-spherical particle a *set of points* on its surface) to extract meaningful local information in a quasi-two-dimensional system of granular rods. In addition, we illustrate how it can be applied to arbitrarily shaped particles such as an assembly of honey bees or pedestrians for obtaining structural information. Details on the implementation of this algorithm with the strategy of balancing computational cost and accuracy are discussed. Furthermore, we provide our python code as open source in order to facilitate Set Voronoi calculations in two dimensions for arbitrarily shaped objects.

## 1 Introduction

Particulate systems are ubiquitous in nature, industry and our daily lives, ranging from active ones like pedestrians or animals, as in Fig. 1, to passive ones such as athermal granules. They all share the characteristics that the macroscopic behavior

---

Simeon Völkel

University of Bayreuth, Experimental Physics V, Universitätsstraße 30, 95447 Bayreuth, Germany,  
e-mail: simeon.voelkel@uni-bayreuth.de

Kai Huang

Duke Kunshan University, Division of Natural and Applied Sciences, No. 8 Duke Avenue, Kunshan,  
Jiangsu, China 215316, e-mail: kai.huang186@dukekunshan.edu.cn &  
University of Bayreuth, Experimental Physics V, Universitätsstraße 30, 95447 Bayreuth, Germany

**Fig. 1** Carniolan honey bees on a partially sealed honeycomb. The Set Voronoi tessellation (black) is based on multiple points (white) per bee.



depends on the arrangement of individual particles relative to each other. Prominent collective effects regarding the dynamics of granular materials, such as the solid-liquid-like transition [1, 2, 3, 4, 5, 6, 7, 8] and pattern formation [9, 10, 11], are typically triggered by the mobility of individual particles. Moreover, there also exists evidence showing that the strain field associated with local rearrangement of particles can be used to obtain the local stress field, which in turn can provide indispensable hints on the establishment of local force networks during jamming transition [12, 13, 14]. Investigations on granular systems thus often rely on accurate measurements of properties such as local volume fraction, neighborhood, etc. For defining these quantities, it is expedient to attribute to every particle a portion of the available space, that “belongs to” or “is occupied” by a single particle.

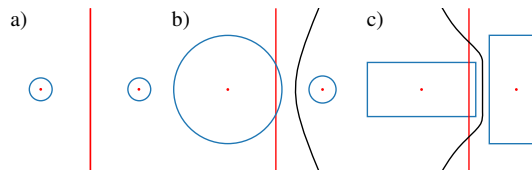
## 2 Limitations of the classical Voronoi tessellation

The honeycomb in Fig. 1 can be seen as an example of a naturally formed tessellation, optimized to have a fair distribution of space for individual larvae of bees to grow inside. Motivated by such self-organized processes in nature, the concept of spatial tessellation was established long time ago [15, 16, 17, 18] in order to analyze structures of various systems in diverse disciplines, from the structure of the universe in astronomy [15] through positioning public schools or post offices in urban planning [19] to characterizing topological aspects of molecular structures [20, 21, 22].

A generic, parameterless approach to attribute space based on a single point per object (typically its center) is the Voronoi tessellation (VT), also known as Dirichlet tessellation, Thiessen polygons or Wigner-Seitz cells [16, 17, 23, 24].

For mono-disperse spherical particles (as well as point-like particles), classical VT based on the particle centers is applicable and delivers intuitive results (see Fig. 2a). This, however, is not the case for polydisperse packings (see Fig. 2b)

**Fig. 2** Comparison of classical VT based on the center (red) of particles and Set VT (black) considering the border of the two particles (blue).



or non-spherical particles (see Fig. 2c). Here, part of the particle on the left lies outside of the Voronoi cell, contributing to an obvious source of error. To overcome this, various weighted Voronoi diagrams have been proposed (see, e. g., [18] for an overview) and implemented in physics and material science [25, 26].

Problems due to applying classical VT to a glass composed of *differently sized* (but spherical) atoms have already been discussed [26]. Here, we highlight the problems arising from applying classical VT to equally sized, but *elongated* particles.

### 3 Set Voronoi algorithm and implementations

A generic way to attribute space to both differently sized particles and non-spherical particles is to tessellate space according to the distance to the closest *surface* (as opposed to center). This can be seen as the limiting case of a classical VT, when considering for each particle the *set of points* marking its surface. Therefore it is also referred to as *Set Voronoi* diagram [27]. The resulting, intuitive cell-borders of the examples in Fig. 2 are depicted in black. Note that the Set Voronoi border for nonoverlapping monodisperse spheres (or circular discs in two dimensions) like in Fig. 2a coincides with the classical Voronoi cell border. Voronoi diagrams with lines and arcs as generators have been studied systematically since the late 1970s [18]. Nevertheless, their importance in the realm of granular physics was rarely realized until the past decade [28, 27, 29, 30].

Recently, Weis & Schönhöfer [31] provided a program based on the Voro++ library [32] to calculate the Set VT, targeting reconstructed CT-scans of three-dimensional (3D) packings of non-spherical granular particles [30]. However, an urgent demand for a solution in two dimensions remained, as it is computationally not economic to apply the 3D algorithm directly to two-dimensional (2D) systems [33]: Adding dimensions to the problem inevitably increases the computational cost for obtaining the tessellation, letting aside the efforts now required to treat the borders in the added dimension(s). Considering as well the fact that many particulate problems of practical interest (e. g., dynamics of pedestrians, flocks or monolayers of granulates) can be treated (quasi-) two-dimensionally and very often data is acquired using 2D imaging techniques, we implemented the Set VT strategy based on discrete points put forward by Schaller et al. [27] in 2D. Our implementation uses the python scripting language together with scipy/numpy libraries [34], relying on VT routines provided by the Qhull library [35]. It is available as free open source software [36].

### 4 Granular rod monolayer as a test case

As an example, we demonstrate the advantages of Set VT using a monolayer of monodisperse granular rods of length  $l = 15$  mm and diameter  $d = 3$  mm. They are confined in a horizontal cylindrical container of diameter  $D = 19$  cm, which is

subjected to sinusoidal vibrations against gravity with oscillation frequency  $f$  and dimensionless acceleration  $\Gamma$  as two control parameters to keep the rods mobilized. More details on the experimental set-up and image analysis procedure can be found in [37]. Depending on the packing density, the rods may organize themselves into an uniaxial nematic state with two-fold rotational symmetry or tetratic state with 4-fold symmetry. For analyzing the disorder-order transition quantitatively, an accurate determination of the local packing density is desired. For amorphous media, such as a random packing of granular particles, (Set) VT provides a direct route to the local area or volume fractions of individual grains [38, 39, 27].

Fig. 3 compares the outcome of classical and Set VT based on a snapshot reconstructed from the positions and orientations obtained experimentally in [37]. This particular snapshot is chosen, as it consists of both dense and dilute regions. The classical VT does not include walls and leads to cells cutting the walls of a container (red solid lines crossing the gray area in Fig. 3a) or even extending to infinity (red dashed lines in Fig. 3a). These problems can be easily and consistently avoided using Set VT, as the container can be included as an additional ‘particle’, naturally limiting the cells of all contained particles (see Fig. 3b). Additionally Set VT delivers a much more reasonable tiling in the sense that no particle cuts its cell’s border, as the container lid prohibits the ‘hard’ rods from overlapping. Quantitatively, the local packing density  $\phi = A_p/A_c$  derived from the projected area of the particles  $A_p = l \cdot d$  and the area of the corresponding cell  $A_c$  obtained from the space tiling also demonstrates the difference clearly: Cells with ‘impossible’  $\phi > 1$  (see color code) disappear and large fluctuations of  $\phi$  for rods aligned with each other in a similar local configuration diminish as Set VT is implemented.

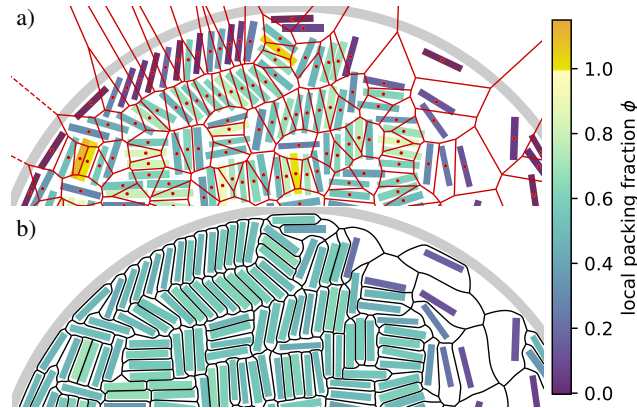


**Fig. 3** VT (a) and Set VT (b) of partly ordered granular rods in quasi-two-dimensions. The parameters are: particle number  $N = 400$ , driving frequency  $f = 50$  Hz and dimensionless acceleration  $\Gamma = 6.26$ . The color code indicates the local packing fraction  $\phi$  according to the different tessellations: classical VT considering the particle centers (red, upper panel) vs. Set VT (black, lower panel) including the container rim as additional particle.

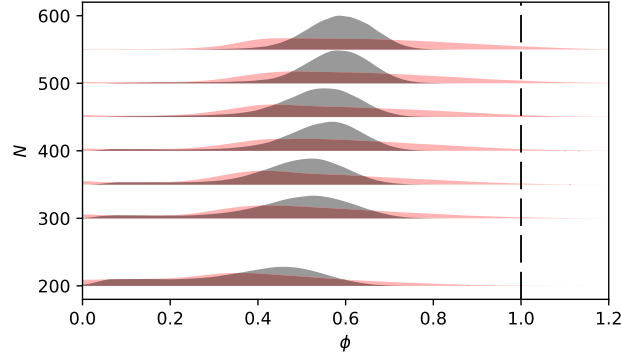


**Fig. 4** Probability density  $P_\phi$  of the local packing fraction  $\phi$  for different numbers of particles  $N$  in the container, obtained from kernel density estimation. Light red and dark gray curves correspond to classical and Set VT, respectively. The peak acceleration is kept in the range  $\Gamma \in [1.94; 20.59]$  and  $f = 50$  Hz is fixed. Other experimental parameters are the same as in Fig. 3. The reflection method [41, 42] has been used to correct for  $\phi$  being non-negative by definition, and the bandwidth of the Gaussian kernel is chosen according to Scott's rule [43] as  $\sigma \cdot n^{-1/5}$  proportional to the standard deviation  $\sigma$  of the distribution and dependent on the number of rods  $n$  (here  $1.7 \times 10^5$  to  $5.3 \times 10^5$  per stacked plot). Captured frames with detection problems (particles (partially) outside of the container, overlapping or of zero size) were skipped to avoid bias.

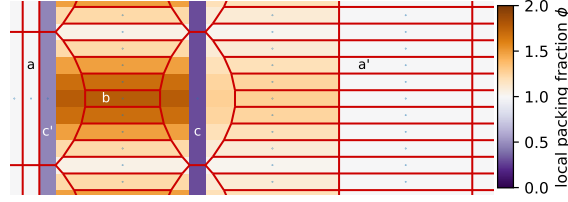
Fig. 4 compares the local packing density distribution obtained from VT (red) and Set VT (black) for different global packing densities. For Set VT, the probability density  $P_\phi$  shows a clear trend of an increasing local packing density with the global one. This feature is much less obvious for the classical VT. There, the most striking observation is the tail of the distribution towards large  $\phi$  becoming more prominent. The dashed line at  $\phi = 1$  marks the upper bound for hard particles and a reasonable tiling. All red curves clearly exceed this limit. This manifests again the importance of observing the applicability of each tessellation technique.

## 5 Why Set Voronoi is essential for elongated particles

To analyze quantitatively the maximal error introduced by applying the classical VT to elongated particles, we consider a perfect, dense packing of identical “hard” rectangles. With no space left between the non-overlapping rectangles, a constant local packing fraction equal to the global packing fraction of unity is expected.

Fig. 5 gives an example for such a dense packing of rectangles with width-to-length ratio  $\varepsilon$ . Classical VT (red lines) gives the expected value for the local packing fraction, as indicated by the color code, if all neighboring particles are aligned in the same direction (cf. particles a and a' in Fig. 5) but fluctuates significantly where rectangles of different orientation come together. Here, local packing fractions up to  $\phi_{VT,max} = 2/(1 + \varepsilon)$  are obtained, e. g., for particle b in Fig. 5. This overestimation is thus a

**Fig. 5** Local packing fraction (see color code) according to classical VT (red lines, based on particle centers) in a dense packing of rectangles with  $\varepsilon = 1/8$  exhibiting tetratic ordering.



first order effect in terms of  $\varepsilon$ . It can reach a remarkable error of 100 % for vanishing width-to-length ratio, even when letting aside any experimental inaccuracies or elasticity of the particles. At the same time, the local packing fraction for neighboring particles  $c$  and  $c'$  in Fig. 5 is underestimated, up to an equally dramatic extent as  $\varepsilon \rightarrow 0$ . Even for a *dense* packing of hard particles (global packing fraction of unity) and without boundary effects, classical VT can indicate *vanishing* local packing fraction, deviating disastrously from the expected value!

On the contrary, Set VT gives consistent local packing fractions. It delivers a value of  $\phi_{\text{Set VT}} = 1$  for every rectangle in Fig. 5 within the numerical uncertainty arising from the approximation of the surface through a finite number of points.

## 6 Performance vs. quality trade-off via erosion

For closely spaced particles special care is required to identify their surface properly before applying the Set VT. For rounded particles with a finite minimal curvature radius  $r_c$ , Schaller et al. [27] show that it is highly beneficial to consider the maximally eroded surfaces, having the constant minimal distance  $r_c$  to the original ones: Using the eroded surface, dramatically fewer points suffice for obtaining the same Set VT and accuracy. In addition, erosion can resolve slight particle overlap. This is particularly helpful for densely packed particles close to jamming [44] and is expected to make investigations of deformable particles feasible [27].

For the granular rods discussed above, the rectangles seen by the camera have sharp corners. In other words,  $r_c = 0$ , preventing a ‘lossless’ erosion. Accurately capturing the sharp corners commands a vanishing erosion depth, which in turn dictates a very close spacing of the discretization points on the eroded surface. As describing a surface with a larger number of points inevitably increases the computational costs, a compromise between accuracy and speed has to be found. Here, we erode the rods by one pixel to remove slight overlap due to finite experimental resolution, detection accuracy and finite elasticity of the particles. Setting the maximum distance between discretization points to the erosion depth delivers satisfactory results and we recommend this as a rule of thumb.

For many systems, however, the situation is more pleasant, especially if the most important property is the elongation, while the dimensions along the other direction(s) are equal and the exact shape of each particle only plays a tangential role, like in the case of the bees shown in Fig. 1. In such a case, it is typically acceptable

to approximate the particle as spherocylinder. This approximation paves the way to a very efficient representation of the particle when using Set VT: The maximally eroded ‘surface’ of each particle is then just its medial axis, a one-dimensional line segment. Furthermore, according to the rule of thumb, one discretization point per radius of the spherocylinder  $r$  suffices for satisfactory results even at high packing densities. For the bees on the honeycomb, this translates to a single digit number of discretization points, each depicted as a white dot in Fig. 1. Nevertheless, this is sufficient for resolving the most prominent and important effects due to the elongated shape of the individual bee, as the black Set Voronoi cell borders illustrate.

As similarly sized rod-shaped particles represent a diverse class of systems, from liquid crystal molecules at a microscopic scale to pedestrians viewed from the top (i. e., when taking their shoulders into account), the above analysis demonstrates that it is essential to employ Set VT for elongated particles.

## 7 Conclusion

Using dynamics of a granular rod monolayer as an example, we demonstrate that Set VT provides a more meaningful tiling of space in comparison to the classical VT that relies on the center of particles. From polydisperse systems to irregularly shaped or even deformable particles, the Set VT algorithm is expected to be substantially more consistent in characterizing the geometric and topological features of particulate systems, many of which can be approximated as elongated particles.

Note that in addition to obtaining the local packing density, VT can also be used to extract other order parameters, such as determining neighbors of individual particles. The Delaunay triangulation, which connects particle centers to their neighbors, follows the natural definition that neighbors share a part of a Voronoi cell border and is a typical approach after classical VT. The extension of this definition to Set VT is straightforward and can be used in further characterizations, for instance, using the bond orientational order parameter [5]. How to extract more meaningful information from Set VT in addition to the local packing density and the improvements against the classical VT will be a focus of future investigations.

**Acknowledgements** We gratefully acknowledge helpful discussions with Simon Weis, Matthias Schröter, Ingo Rehberg, Stefan Hartung and Wolfgang Schöpf. We thank Alexander and Valentin Dichtl for the possibility of taking the picture of the bees in Fig. 1 during an inspection of the hive. This work is supported by the German Research Foundation (DFG) under Grant No. HU1939/4-1.

## References

1. K. Huang, C. Krülle, I. Rehberg, J. Appl. Math. Mech. **90**(12), 911 (2010). DOI 10.1002/zamm.201000110
2. K. Huang *et al.*, Phys. Rev. E **79**(1), 010301 (2009). DOI 10.1103/PhysRevE.79.010301

3. K. Huang, K. Röller, S. Herminghaus, *Eur. Phys. J. Special Topics* **179**(1), 25 (2009). DOI 10.1140/epjst/e2010-01191-5
4. B. Andreotti, Y. Forterre, O. Pouliquen, *Granular Media: Between Fluid and Solid* (Cambridge University Press, 2013)
5. C. May *et al.*, *Phys. Rev. E* **88**(6), 062201 (2013). DOI 10.1103/PhysRevE.88.062201
6. S.C. Zhao, M. Schröter, *Soft Matter* **10**(23), 4208 (2014). DOI 10.1039/C3SM53176G
7. P. Ramming, K. Huang, *EPJ Web Conf.* **140**, 08003 (2017). DOI 10.1051/epjconf/201714008003
8. M. Baur, K. Huang, *Phys. Rev. E* **95**(3), 030901 (2017). DOI 10.1103/PhysRevE.95.030901
9. G.H. Ristow, *Pattern Formation in Granular Materials* (Springer, 2000)
10. A. Fortini, K. Huang, *Phys. Rev. E* **91**(3), 032206 (2015). DOI 10.1103/PhysRevE.91.032206
11. A. Zippelius, K. Huang, *Sci. Rep.* **7**(1) (2017). DOI 10.1038/s41598-017-03844-0
12. A.J. Liu, S.R. Nagel, *Nature* **396**(6706), 21 (1998). DOI 10.1038/23819
13. D. Bi *et al.*, *Nature* **480**(7377), 355 (2011). DOI 10.1038/nature10667
14. Y. Zhao *et al.*, *Phys. Rev. Lett.* **123**, 158001 (2019). DOI 10.1103/PhysRevLett.123.158001
15. R. Descartes, *Principles of Philosophy* (Amsterdam, 1644). 3-7873-1697-3
16. G. Dirichlet, *Journal für die reine und angewandte Mathematik* (40), 209 (1850)
17. G. Voronoi, *Journal für die reine und angewandte Mathematik* (133), 97 (1907)
18. A. Okabe *et al.*, *Spatial Tessellations: Concepts and Applications of Voronoi Diagrams*, 2nd edn. (John Wiley & Sons, Ltd, 2000). DOI 10.1002/9780470317013
19. M. McAllister, D. Kirkpatrick, J. Snoeyink, *Discrete Comput. Geom.* **15**(1), 73 (1996)
20. A.L. Mackay, *J. Molec. Struct.* **336**(2), 293 (1995). DOI 10.1016/0166-1280(95)04172-3
21. F. Aurenhammer, *ACM Comput. Surv.* **23**(3), 345 (1991). DOI 10.1145/116873.116880
22. J. Bernauer *et al.*, *Bioinformatics* **24**(5), 652 (2008). DOI 10.1093/bioinformatics/btn022
23. A.H. Thiessen, *Mon. Weather Rev.* **39**(7), 1082 (1911). DOI 10.1175/1520-0493(1911)39<1082b:PAFLA>2.0.CO;2
24. E. Wigner, F. Seitz, *Phys. Rev.* **43**, 804 (1933). DOI 10.1103/PhysRev.43.804
25. J. Park, Y. Shibutani, *Intermetallics* **15**(2), 187 (2007). DOI 10.1016/j.intermet.2006.05.005
26. J. Park, Y. Shibutani, *Intermetallics* **23**, 91 (2012). DOI 10.1016/j.intermet.2011.12.019
27. F.M. Schaller *et al.*, *Philos. Mag.* **93**(31-33), 3993 (2013). DOI 10.1080/14786435.2013.834389
28. A. Baule *et al.*, *Nat. Commun.* **4**(1), 2194 (2013). DOI 10.1038/ncomms3194
29. A. Baule, H. A. Makse, *Soft Matter* **10**(25), 4423 (2014). DOI 10.1039/C3SM52783B
30. S. Weis *et al.*, *EPJ Web Conf.* **140**, 06007 (2017). DOI 10.1051/epjconf/201714006007
31. S. Weis, P. Schönhofer. Pomelo: calculate generic set voronoi diagrams with c++11 (2017). URL <http://theorie1.physik.fau.de/research/pomelo/index.html>
32. C. Rycroft, Voronoi++: a three-dimensional Voronoi cell library in C++. *Tech. Rep. LBNL-1432E*, 946741 (2009). DOI 10.2172/946741
33. S. Weis. private communication
34. P. Virtanen *et al.* (SciPy 1.0 Contributors), arXiv e-prints arXiv:1907.10121 (2019)
35. C.B. Barber *et al.*, *ACM Trans. Math. Softw.* **22**(4), 469 (1996). DOI 10.1145/235815.235821
36. S. Völkel. setvoronoi2d: Calculate the Set Voronoi tessellation in two dimensions. online. DOI 10.5281/zenodo.3531546
37. T. Müller *et al.*, *Phys. Rev. E* **91**(6), 062207 (2015). DOI 10.1103/PhysRevE.91.062207
38. C. Song, P. Wang, H.A. Makse, *Nature* **453**(7195), 629 (2008). DOI 10.1038/nature06981
39. S. Torquato, F.H. Stillinger, *Rev. Mod. Phys.* **82**(3), 2633 (2010). DOI 10.1103/RevModPhys.82.2633
40. O. Tange, *GNU Parallel 2018* (Ole Tange, 2018). DOI 10.5281/zenodo.1146014
41. B. Silverman, *Density Estimation for Statistics and Data Analysis*. Monographs on Statistics & Applied Probability (Chapman & Hall, 1986)
42. L.I. Boneva, D. Kendall, I. Stefanov, *J. Royal Stat. Soc. B* **33**(1), 1 (1971). DOI 10.1111/j.2517-6161.1971.tb00855.x
43. D.W. Scott, *Multivariate density estimation: theory, practice, and visualization*, 2nd edn. (Wiley, Hoboken NJ, 2015). DOI 10.1002/9781118575574
44. I. Zuriguel *et al.*, *Sci. Rep.* **4**, 7324 (2014). DOI 10.1038/srep07324